J Sol-Gel Sci Technol (2008) 46:313–322
DOI 10.1007/s10971-007-1661-4

ORIGINAL PAPER

Light-activated functional mesostructured silica

Erik Johansson · Eunshil Choi · Sarah Angelos · Monty Liong · Jeffrey I. Zink

Received: 30 August 2007 / Accepted: 19 November 2007 / Published online: 19 December 2007

Abstract Mesostructured silica thin films and particles provide highly versatile supports or frameworks for functional materials where a desired function (such as energy transfer, electron transfer, or molecular machines) is induced by molecules deliberately placed in specific regions of the structure. The relatively gentle templated sol–gel synthesis methods allow a wide variety of molecules to be used, and the optical transparency of the framework is very suitable for studies of light-induced functionality. In this paper, three types of functionality are used to obtain fundamental understanding of the materials themselves and to develop active materials that can trap and release molecules from the pores upon command. Photo-induced energy transfer is used to verify that molecules can be placed in specific spatially separated regions of the framework; fluorescence resonance energy transfer is used as a molecular ruler to measure quantitatively the distance between pairs of molecules. Secondly, photo-induced electron transfer is used to obtain fundamental information about the electrical insulating properties of the framework. Finally, two types of molecular machines, a light-driven impeller and a light activated nanovalve, are described. Both machines contain moving parts attached to solid supports and do useful work. The valves trap and release molecules from the mesopores, and the impellers expel molecules from the pores. Applications of the materials to drug delivery and the release of drug molecules inside living cells is described.

Keywords Energy transfer · Electron transfer · Nano machines · Nano valves

E. Johansson · E. Choi · S. Angelos · M. Liong · J. I. Zink (✉)
Department of Chemistry and Biochemistry, University of California at Los Angeles, Los Angeles, CA 90095, USA
e-mail: zink@chem.ucla.edu

E. Johansson
e-mail: lars@chem.ucla.edu

E. Choi
e-mail: echoi@chem.ucla.edu

S. Angelos
e-mail: angelos@chem.ucla.edu

M. Liong
e-mail: mliong@chem.ucla.edu

1 Introduction

Inorganic oxide material synthesis by sol–gel methods has a long history and has been reviewed extensively [1–3]. Functionalization of sol–gel materials can be achieved by incorporating active molecules into the silica framework, in the interior of mesopores, at template-silica interfaces, or on the silica surface. The earliest functional sol–gel materials were obtained by physically immobilizing molecules in the pores. The incorporation of molecules, ranging from simple acid–base indicators to complex biosystems such as enzymes, was and still is an active area of investigation [4–11]. The first report of mesostructured silica, in the form of surfactant templated particles appeared in 1992 [12] and that of mesostructured thin films formed by evaporation induced self-assembly appeared in 1997 [13]. Since then extensive background has developed on the use of surfactants and block copolymers for the self-assembly of metal oxides [14–17]. One-step, one-pot synthetic strategies to deliberately place photoactive molecules in the spatially separated regions of the mesostructure were recently reported [18–21]. In this approach, all of the

components were dissolved in the starting sol, including all dopants. Doped mesostructured films were produced by dip-coating the sol onto a silicon substrate; luminescent molecules were used to probe the film formation [22–25]. The micelle assembly process was monitored and correlated with changes in solvent composition. Probes that were preferentially incorporated in specific regions (such as the micelle interior) were used. In the most recent examples, as will be discussed below, designed simultaneous placement of two or more molecules into two different regions has been demonstrated, and detailed studies of both spectroscopic and dynamic properties have been reported [21, 26].

In this article, we begin by describing the uses of mesostructured silica supports for energy transfer and electron transfer measurements. After a short review of general strategies for deliberate placement of photoactive molecules in the different regions of mesostructured silica, the use of energy transfer between deliberately placed donors and acceptors to measure the spatial separation of molecules is discussed. Next, the use of electron donors and acceptors that were deliberately placed in different regions of mesostructured thin films to determine the value for the electron tunneling decay constant of mesostructured silica is described. Another major application of the silica structure, its use as a framework for molecular machines, is then discussed. Rotaxanes and azobenzenes are attached to mesoporous silica and used as valves and impellers in non-aqueous environments, aqueous environments and cells.

2 Deliberate placement

Sol–gel mesostructured thin films consist of three different regions: the silica framework, the hydrophobic micellar core and the ionic interface that separates them (Fig. 1).

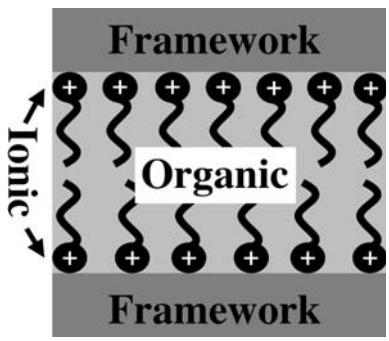

Fig. 1 The three regions of mesostructured thin films templated by ionic surfactants. In this figure a cationic surfactant templates the mesostructure

In order to develop functional mesostructured materials, selective derivitization of the different regions is often required, either during the film formation or after. Both ways of derivatizing the film have their advantages and disadvantages. Derivatization during the film formation has the advantage that all regions of the film are accessible, including the silica framework, the ionic interface and the hydrophobic region. The types of molecules that can be used are limited. They must be soluble in the initial sol and able to withstand the conditions of the initial sol. It should also be noted that incorporation of dopants into the sol can alter the mesostructure of the final film [27]. Post synthesis derivatization has the advantage that once the film is formed it is relatively robust, and therefore a greater range in physical and chemical conditions and solvent properties can be employed. The disadvantage is that some regions of the film, such as the interior of the silica framework, are not easily functionalized because of limited accessibility. Strategies for selectively placing molecules in the different regions of sol–gel thin films are summarized in Table 1.

3 Energy transfer

Energy transfer in mesostructured thin films serves as a good example of the versatility of the placement strategies [21]. Energy donors and acceptors (Scheme 1) were placed in different regions of CTAB-templated mesostructured thin films. Time-dependent and steady state luminescence spectroscopy were used to prove donor- and acceptor placement and verify concentration dependent energy transfer. Fitting of experimental luminescence decay traces using Förster theory gave measurements of minimum donor acceptor distances, proving the spatial separation of donors and acceptors.

Table 1 Strategies for deliberate placement

Strategy	Examples
Philicity	Pyrene as a probe of micelle formation [22, 23]
	Fluorescent nanocomposites [28]
Bonding	Placement of functional molecules in SiO_2 framework [18, 19, 21, 29, 30]
	Construction of framework exclusively from functional molecules [31–33]
Bifunctional	Placement of active molecules bonded to the inside of the pores [18, 19, 21, 29, 34–36]
Post synthesis grafting	Light induced charge separation [37]
Backfilling	Loading of molecules for controlled release [38, 39]
	Incorporation of pyrene into mesoporous silica [40]

Scheme 1 Structures of the energy transfer donors and acceptors

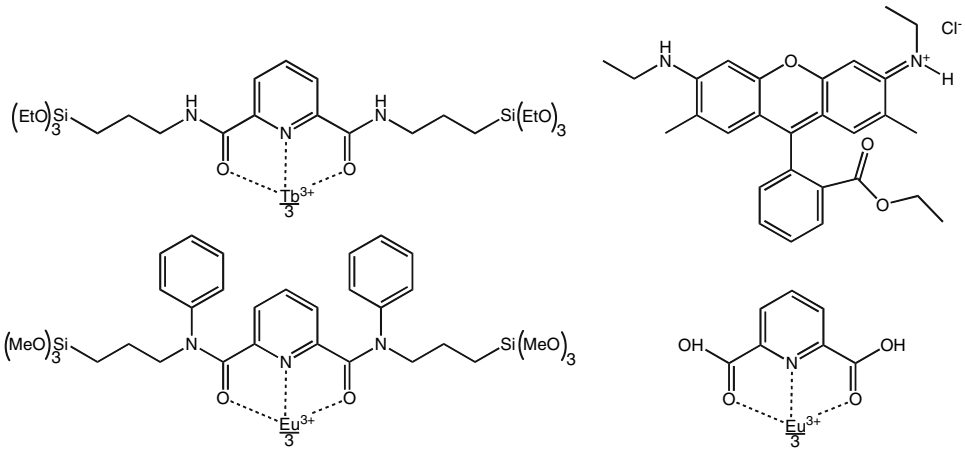

3.1 Verification of donor and acceptor placement

Two placement strategies were employed in order to achieve spatial separation between energy donors and acceptors. The bonding strategy was employed to place the lanthanide complexes, which served as energy donors, in the silica framework. The placement of Rhodamine 6G (R6G) in the organic region was achieved using the philicity strategy. The verification of the placement of R6G was achieved by using fluorescence spectra, excitation spectra and fluorescence lifetime data. Both the luminescence spectra and excitation spectra of R6G were redshifted for the structured films compared to the amorphous films. The redshift is a function of R6G transitioning from a polar to a nonpolar environment [41, 42], in this example from the polar silica region in amorphous films, to the hydrophobic micellar region. Further proof was obtained studying the luminescence lifetime of R6G in mesostructured films as a function of R6G concentration. The trends agreed with those observed in micelles [43]. If the concentration of R6G is high, aggregation might occur. Since the spectral properties of R6G aggregates are different from those of the monomers it is important to be aware of possible aggregation. Aggregation of R6G has been studied on the porous surface of silica gels [44] as well as in mesostructured silica [21]. For these studies of energy transfer in mesostructured silica thin films it was important to be aware of the aggregation concentration-threshold in order to deduce accurate donor–acceptor distances.

Luminescence lifetime studies were used to investigate the location of the lanthanide complexes. Lanthanide complexes are sensitive to their surrounding environment [18, 19]. Luminescence lifetime data in these experiments revealed that the silylated complexes reside in the same environment in amorphous and structured films. Hence, silylated complexes position themselves in the framework.

3.2 Energy-transfer and distance measurements

Luminescence spectra and luminescence lifetime measurements prove that energy transfer does occur. When excited at the absorption maximum of the energy donor, the R6G luminescence intensity increased for all films where the energy donor was present compared to that when the energy donor was absent. The trend was also observed when monitoring the luminescence intensity of the energy donor. A strong dependence of the luminescence intensity on the R6G concentration was observed; increasing the concentration of the energy acceptor, R6G, quenched the donor luminescence. Lifetime measurements also confirmed that energy transfer took place. Monitoring the R6G luminescence lifetime revealed that it increased by as much as three orders of magnitude, to 1.55 μs, in the presence of the energy donor. The R6G luminescence lifetime was longest when there was a large excess of donor compared to acceptor. When increasing the acceptor concentration, quenching of the donor was more efficient which leads to a shorter observed lifetime for R6G.

In order to calculate the distance separating the donor and acceptor, the Förster radius must be on the same order as the distance from the center of the hydrophobic region inside the micelles to the center of the silicate framework. The calculated Förster radius, R_0, of 40 Å, makes this system suitable since the distance from the center of a tube to the middle of the framework is approximately 20 Å, one-half of the *d*-spacing calculated from the XRD pattern.

The energy transfer efficiency, E, was calculated according to Eq. 1.

$$E = \frac{R_o^6}{R^6 + R_o^6} = 1 - \frac{\tau_{DA}}{\tau_D} = 1 - \frac{F_{DA}}{F_D} \quad (1)$$

where E is the calculated quenching efficiency, τ_D and F_D are the lifetime and fluorescence intensity of the donor in the absence of acceptor, and τ_{DA} and F_{DA} are the

corresponding quantities in the presence of acceptor. Experimentally obtained quenching efficiencies together with the Förster radius R_0 of 40 Å were used in order to solve for R in the above equation. Using low concentrations of R6G led to a calculated average donor-acceptor distance of $R = 65$ Å. As the R6G concentration increased, R decreased but did not go below $R = 29$ Å. This demonstrated that the donors and acceptors are indeed spatially separated because they always remain separated by a minimum distance, $R = 29$ Å, which corresponds closely to the separation distance that would be expected based on the dimensions of the mesostructured thin film.

This work showed that energy donors and acceptors were deliberately placed in different regions of mesostructured thin films. The minimum of $R = 29$ Å separation showed that the donors and acceptors are located exclusively in different regions of the mesostructured thin films.

4 Electron transfer [26]

Electron transfer in mesostructured thin films has been studied to measure the insulating properties of the films. Deliberate placement methods were used to position electron donors and acceptors in CTAB-templated mesostructured thin films and to measure the electron tunneling decay constant β for the silica framework region and the contact-quenching rate, k_0, for the donor acceptor pair. An electron donor was placed in the silicate framework using the bonding strategy and an electron acceptor was positioned in the ionic interface using the philicity approach. Spectroscopic measurements were used to confirm the placement and stability of the electron donors and acceptors and to obtain the luminescence decay traces that provided the data for the calculations.

4.1 Deliberate placement methods

Two deliberate placement strategies were used to position the electron donor and acceptor in the silicate thin film. A modified *tris*-(bipyridine) ruthenium(II) dication was placed in the silica framework using the bonding strategy. *Tris*-(4,4′-methoxy 2,2′-bipyridine) ruthenium(II) hexafluorophosphate was reacted with isocyanatopropyl triethoxysilane in order to create the donor, **D**, shown in Scheme 2.

The presence of the six alkoxysilane-terminated arms on **D** forces it to co-assemble with the silica framework, thus becoming a part of it, *vide infra*. The electron acceptor, **A**, shown in Scheme 2, is placed in the ionic interface region using the philicity strategy. **A** is modeled on the well-known electron acceptor methyl viologen, but modified with a hexadecyl tail turning it into a surfactant. Because **A** is a surfactant, the hexadecyl tail will incorporate into the CTAB micelles while the electroactive headgroup will reside in the ionic interface.

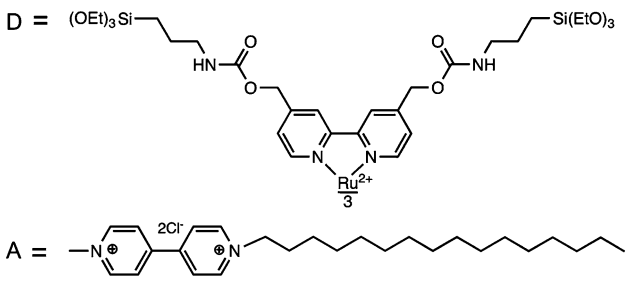

Scheme 2 Structures of the electron donor (D) and acceptor (A)

4.2 Verification of donor and acceptor placement

The placement of **D** was verified using steady state luminescence spectroscopy. Luminescence spectra were obtained of **D** in mesostructured films, non-structured films and the sol. The luminescence spectrum for **D** in the mesostructured film, shown in Fig. 2, is almost identical to that for **D** in an amorphous film. The spectrum of **D** in the sol blue shifted as expected when going from solution to solid [26]. This is due to the absence, in the solid state, of solvent-molecules able to arrange themselves favorably around **D**, decreasing the energy gap between **D** and ***D**. The spectra for the structured film and the amorphous film are identical because the luminescent moiety, **D**, is surrounded by the same environment in both films.

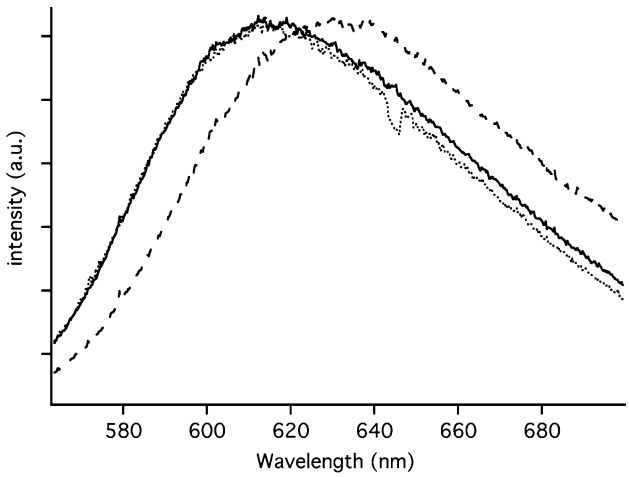

Fig. 2 Luminescence spectra for **D** in structured films (solid), amorphous films (dotted) and the sol (broken line). The spectra are very similar for the structured and non-structured films, but different from that in the sol, signaling that **D** always resides in the silica matrix

The electron acceptor, **A**, has been shown previously to incorporate fully into cationic micelles at surfactant concentrations much lower than those present in mesostructured thin films [45, 46]. **A** is present, and intact, in the thin films as is demonstrated by the concentration dependent quenching effect of **D** luminescence observed when incorporating various amounts of **A** into the films.

4.3 Electron transfer studies

The electron transfer process between **D** and **A** in the mesostructured thin films was investigated by using experimental measurements of the luminescence decay of **D** in the presence and absence of **A**, shown in Fig. 3.

The contact quenching rate, k_0, and the electron tunneling decay constant β were calculated by fitting the experimental luminescence decay traces. Because **D** and **A** are separated in different regions of the structured film, electron transfer is a non-contact process and takes place through tunneling. When electron transfer takes place through tunneling, the transfer rate drops exponentially with the distance separating the donor and acceptor. The rate at which the electron transfer rate between **D** and **A** decreases as a function of distance is described by β. β is a parameter known for many other systems including vacuum, frozen glasses, proteins, and molecular bridges [47–50]. Measurements of electron transfer in silica thin films allow for comparison between the silica framework of the structured thin film and many other systems.

The values of β and k_0 were calculated by using Eq. 2 to fit the experimental data. In the fitting procedure, first the positions of the CTAB headgroups in the mesostructured thin films are determined using the *d*-spacing of the film together with the knowledge that the tubes are arranged in a 2-D hexagonal pattern. From the list of positions of CTAB headgroups are chosen the positions of the viologen headgroups using a random number generator. The position of the donor is then chosen randomly under the constraint that it must be in the silica framework. The seven smallest **D** to **A** distances are then calculated. A physically relevant pair of β and k_0 values is then chosen, which together with the **D** to **A** distances are used to calculate a luminescence decay trace according to Eq. 2. In Eq. 2, $I(t)$ is the luminescence decay trace in the presence of **A**, $I_0(t)$ is the luminescence decay trace in the absence of **A**, R_i is the distance between **D** and acceptor i, and R_0 is the **D–A** shortest distance of electron transfer, when **D** and **A** are in contact.

$$I(t) = I_0(t)\prod_i \exp(-t \times k_0 \times \exp(-\beta(R_i - R_0))) \qquad (2)$$

The calculated trace is compared to that experimentally obtained and the "goodness" of the fit is determined by the variance, S. The variance is stored in a vector together with the β and k_0 pair used. This is repeated for all physically relevant combinations of β and k_0. The generated contour plot, where β and k_0 are the x and y-axis respectively and S is the altitude, is used to find the β and k_0 value corresponding to the best fit. The best fit is recorded together with the β and k_0 pair associated with it.

The obtained value of k_0 is $k_0 = 1 \times 10^{(13.5\pm0.8)}$ s^{-1}. A previous study that measured k_0 for *tris*-(bipyridine) ruthenium(II) linked to methyl viologen via a methyl group obtained a quenching rate $k = 2.5 \times 10^{11}$ s^{-1}. The electron transfer rate that was obtained (2.5×10^{11} s^{-1}) is lower than the calculated k_0, which is expected since the donor and acceptor are not in direct contact but held apart by a CH_2 group. β can neither be less than zero nor can it be greater that 4 Å^{-1} which is the value obtained in vacuum. Our calculated value of $\beta = 2.5 \pm 0.4$ Å^{-1} shows that silica is a good insulator. β is an important parameter known for a wide variety of systems such as molecular bridges, frozen glasses, proteins and vacuum (Fig. 4).

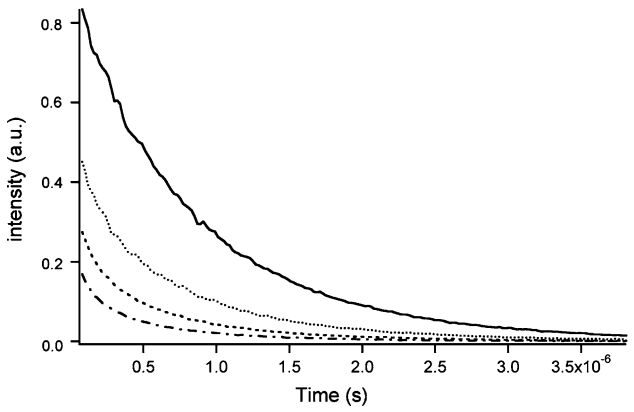

Fig. 3 Luminescence decay traces for D in the presence of varying concentrations of A (increasing concentration of **A** from top to bottom)

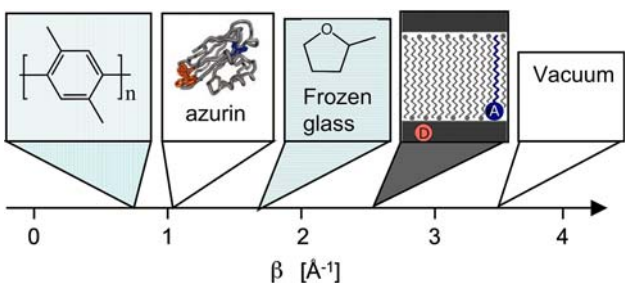

Fig. 4 Comparison of β for different systems

Table 2 Controlled release motifs and modes of activation

Controlled release motif	Mode of activation	References
Pseudorotaxane-based nanovalves	Redox, competitive binding, pH, light	[51–56]
Rotaxane-based nanovalves	Redox	[39, 55]
Azobenzene nanoimpellers	Light	[38]
Chemically removable caps	Reduction, light	[57]

5 Molecular machines

Mesostructured silica nanoparticles are very useful as frameworks and reservoirs for valves and impellers to control the release of molecules from the pores. These materials have been used as supports for controlled release applications together with many types of valves. The valves employed are molecular machines; they are molecular moving parts that perform specific functions. Table 2 lists various molecular machines used in conjunction with mesostructured silica supports.

5.1 Rotaxane and pseudorotaxane based nanovalves

Controlled release of guests from mesostructured silica nanoparticles has been accomplished using supramolecular nanovalves constructed from [2]rotaxanes and [2]pseudorotaxanes [39, 51–55]. When these machines are positioned on the surface of nanoparticles, the $CBPQT^{4+}$ rings encircling the BHEEEN threads are able to gate the entrances to mesopores and the valves are closed. The movement of the rings away from the pore opening can be induced by reducing agents such as $NaCNBH_3$ to unblock the pore entrances and open the valves (Fig. 5).

The versatility of this redox active nanovalve was demonstrated by reconfiguring the system for light activation [55]. Photosensitizers that are powerful reductants in their photo-excited states are capable of reducing the $CBPQT^{4+}$ rings to cause the movement. By attaching them to the surface of the nanoparticles, a photo-induced electron transfer reduced the ring and activated the valve. Specifically, 9-anthracenecarboxylic acid (ACA) and $Ru^{II}(bpy)_2(bpy(–CH_2OH)_2$ were used as photosensitizers. Upon irradiation with the appropriate wavelength of light (351 nm for ACA, 457 nm for $Ru(bpy)_3$), the excited photosensitizer transferred an electron to a nearby $CBPQT^{4+}$ ring to induce dissociation and open the nanovalve (Fig. 6). In order to prevent electron transfer back from the $CBPQT^{3+}$ ring to the oxidized photosensitizer a sacrificial reducing agent, triethanolamine, is used. Triethanolamine prevent the back electron transfer by reducing the oxidized photosensitizer as can be seen in Eq. 3a–c.

$$\text{Photosensitizer} \xrightarrow{h\nu} \text{Photosensitizer}^{*} \tag{3a}$$

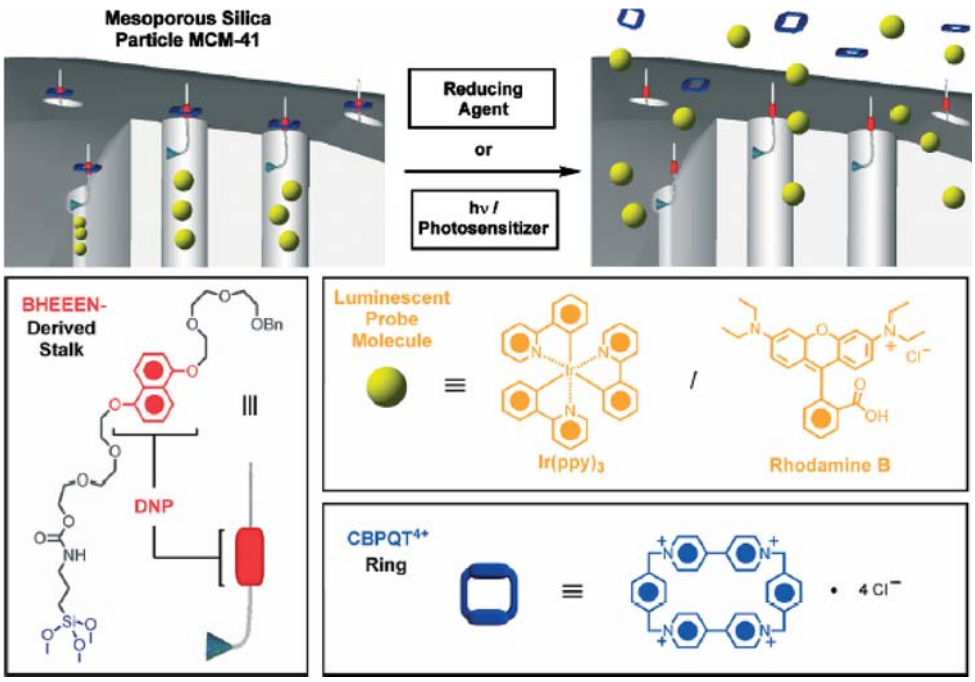

Fig. 5 The source of energy used to operate the machine is light and thus enables the machine to be operated by remote control. Photo-induced electron transfer, between the donor and the moving acceptor, causes the chemical changes that open the valve

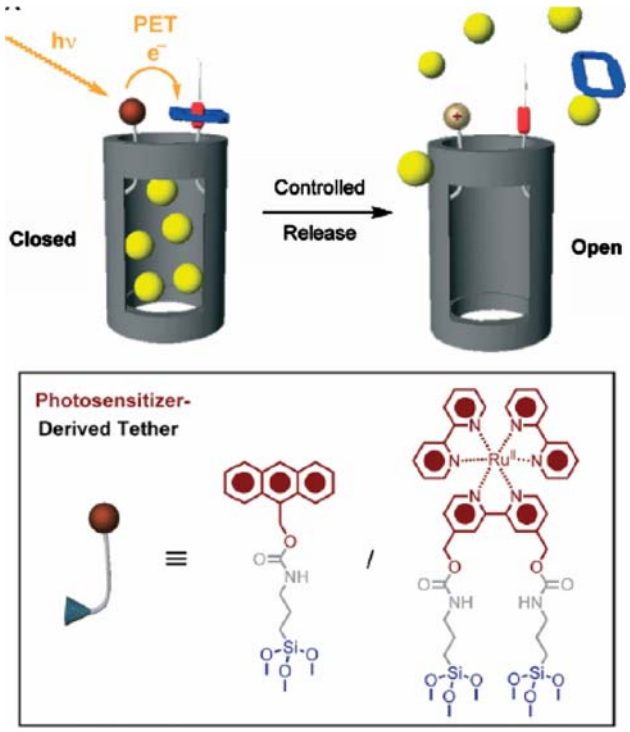

Fig. 6 Proposed mechanism for operation of light activated nanovalve

$$\text{Photosensitizer}^{*} + \text{CBPQT}^{4+} \longrightarrow \text{Photosensitizer}^{+} + \text{CBPQT}^{3+} \quad (3b)$$

$$\text{Photosensitizer}^{+} + \text{Triethanolamine} \longrightarrow \text{Photosensitizer} + \text{Products} \quad (3c)$$

The source of energy used to operate the machine is light and thus enables the machine to be operated by remote control. Photo-induced electron transfer, in this case between the donor and the moving acceptor, through the intervening solvent causes the chemical changes that open the valves.

5.2 Photophysics of azobenzene motion in nanopores

On-command release of molecules from mesoporous silica nanoparticles can be realized by means other than using nanovalves attached to the outside of MSNs. The use of azobenzenes as light activated impellers for releasing molecules is described below.

Azobenzene-functionalized mesoporous inorganic materials have attracted significant attention [58–60]. Detailed investigations into azobenzene *cis/trans* isomerization in mesostructured silica were recently reported [35]. Both 2-D hexagonal mesostructured silica thin films and MCM-41-type silica powders were investigated. Azobenzenes were positioned in the pore interior, with one end bonded to the pore wall and the other end, derivatized with generation zero (AzoG0) to three (AzoG3) (Fig. 7) of the *Fréchet* Dendron, free to undergo large amplitude photo-driven motion.

The bifunctional strategy was used to position the isocyanatosilane derivatized azobenzene [61, 62]. The templating surfactant was removed using acidic methanol, after which the azobenzene *cis/trans* isomerization was studied using luminescence spectroscopy.

The thermal *cis* to *trans* isomerization rate constant in solution is similar for all generations of the azobenzene derivatives ($k = 3.3 \times 10^{-6}\ \text{s}^{-1}$ for generation zero to $k = 2.6 \times 10^{-6}\ \text{s}^{-1}$ for generation three) and can be understood as the small terminus of the molecule moving because it is almost the same for all of these azo molecules. Large changes in the rate constants for the thermal *cis* to *trans* isomerizations of the azo derivatives were observed in the series of small ($k = 1.02 \times 10^{-5}\ \text{s}^{-1}$) to the large molecule ($k = 2.6 \times 10^{-6}\ \text{s}^{-1}$). These changes indicate that the dendrimer is moving and there is a clear effect on the rate-constant caused by the size of the dendrimer.

5.3 Photo-responsive nanoimpellers

Building on the photophysical studies, a photo-driven controlled release system based on azobenzenes was developed (Fig. 8) [38].

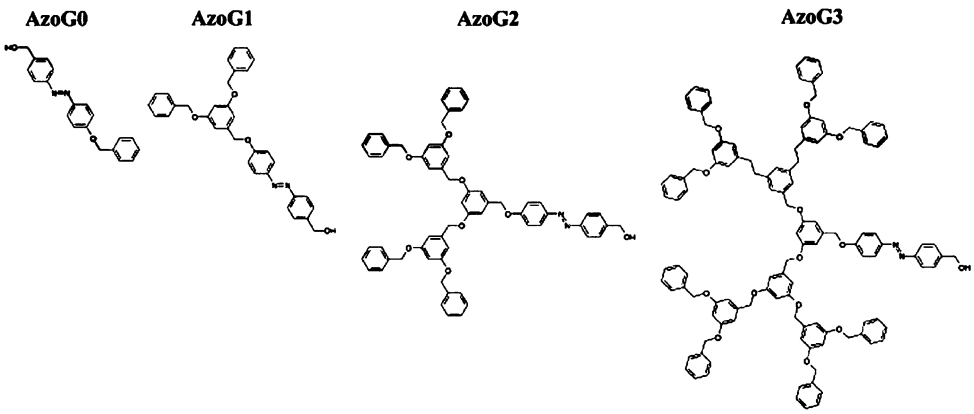

Fig. 7 Chemical structures of the azobenzene molecules from generation zero (AzoG0) to three (AzoG3) of the *Fréchet* Dendron

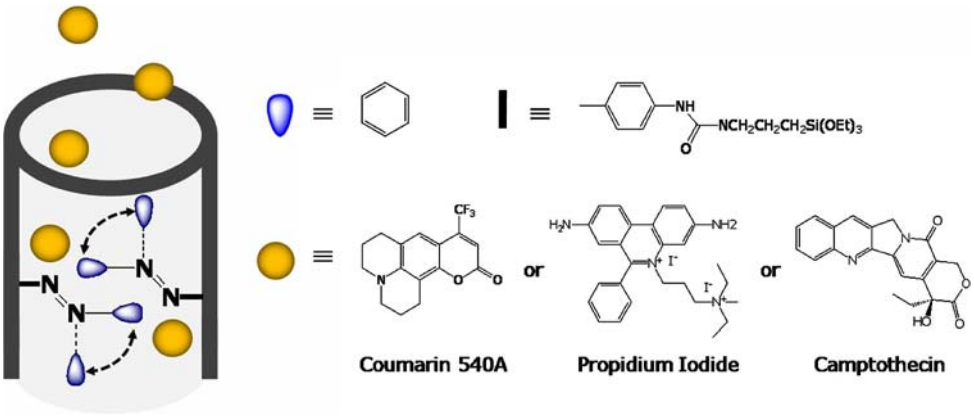

Fig. 8 Mesoporous silica nanoparticles functionalized with azobenzene derivatives and release of pore contents from the particles by the back-and-forth wagging motion of the photo-activated azobenzenes

The azobenzene-derivatized mesoporous silica nanoparticles were filled with either coumarin 540 (C540) or Rhodamine 6G (R6G) and placed in a cuvette filled with methanol. The photo-driven expulsion of the dye molecules from the pores was monitored by fluorescence spectroscopy. The fluorescence intensities of the released probes at the emission maximum (540 nm for C540 and 562 nm for R6G) were monitored as a function of time. When the particles were irradiated with 457 nm light where both azobenzene conformers absorb, the dyes were expelled from the pores and the increase of fluorescence in solution was recorded while negligible release of molecules were detected from unexcited particles.

The dynamic wagging motion of the azobenzene machines probably drives the photo-controlled release of molecules from the particles. Under 457 nm illumination, the continuous isomerization of two conformers occurs reversibly, stimulating the untethered azobenzene terminus to move back and forth and expelling the loaded molecules from the pores. On the other hand, dye molecules are trapped in the pores in the absence of light activation because the static azobenzene machines congest the inner pore channels and prevent the escape of molecules.

6 Drug delivery

The logical step following successful release of probe molecules in a test system is to modify the system so that it can be used for controlled release under biological conditions. This means that the particles must be compatible with cells as well as have desired properties under physiological conditions. Mesoporous silica nanoparticles have several advantageous features over other nanoparticle-based drug delivery systems for use in the delivery of drugs. The porous interiors of the materials are highly suitable for storing drug molecules. The pore size and environment can be modified to selectively store different molecules of interest [63, 64], while the size and shape of the nanoparticles can be tuned to enhance the cellular uptake process [62]. These inorganic materials are stable and can withstand varying pH conditions [65]. Modification of mesoporous silica nanoparticles using the bifunctional strategy, post-synthesis grafting, and backfilling strategy in order to make them suitable for drug delivery applications was recently reported [66]. The modified nanoparticles were able to deliver the water-insoluble drug camptothecin into different types of human cancer cells.

To create an effective intracellular drug delivery system, the particles have to be small enough to enter cells, be well-dispersed in buffered aqueous solution, and contain pores that can store the drug molecules. The synthetic method for the nanoparticles used a dilute precursor solution, high temperature, base catalysis, and CTAB as the mesostructure template [67–69]. In order to monitor the nanoparticles inside the cells, fluorescein isothiocyanate dye molecules were conjugated and attached along the pore walls using the bifunctional strategy. The surface of the nanoparticles was derivatized with hydrophilic phosphonate groups by post-synthesis grafting to prevent the nanoparticle aggregation [70, 71].

Delivery of anticancer drugs into living cells on demand using azobenzene derivatized nanoparticles ($\sim$350 nm in diameter) was successful [72]. It was demonstrated that the intracellular release of guest molecules was sensitized by light excitation of the azobenzenes. In this study, the particles were templated by dodecyltrimetylammonium bromide (DTAB), which templated a smaller pore size and thus minimized the leakage of the system in the dark. Nitrogen sorption isotherm analysis of the particles indicated a BJH average pore diameter of 1.9 ± 0.1 nm, BET surface area of 621.19 $m^2\ g^{-1}$, and total pore volume of 0.248 $cm^3\ g^{-1}$. Intracellular controlled release of the drug molecules was tested in vitro using the azobenzene-derviatized particles containing $\sim$0.6 wt% of the drugs in the mesopores. The PANC-1 cancer cells were treated with a suspension of the particles loaded with a membrane-impermeable cell staining

dye, propidium iodide (PI). After 3 h incubation, the cells were washed with buffer to remove the particles that were not taken up by the cells. The cells containing the dye-loaded particles were either left in the dark or irradiated for 5 min with a laser light at different wavelengths, and then examined by confocal microscopy ($\lambda_{ex} = 337$ nm). Fluorescent images of the cells show that the PI dye molecules were released from the particles and stained the cell nuclei when the impellers were excited (Fig. 9a). When the treated cells were irradiated with 413 nm light, a wavelength that stimulates continuous *cis/trans* isomerization, the cell nuclei were stained red. On the other hand, only a slight amount of staining of the nuclei was observed on the cell samples that were kept in the dark. No staining of the cells was observed when they were irradiated with 676 nm light, a wavelength that the azobenzene molecules do not absorb.

When cells were loaded with particles containing the anticancer drug camptothecin (CPT), apoptosis was induced using light stimuli (Fig. 9b). In the absence of light stimuli, the CPT remained inside the particles and the cells were not damaged. Illumination, however, promptly expelled the drug molecules from the particles, which induced nuclear fragmentation and cell death. For the fluorescence imaging, the irradiated cells were double-stained with a 1:1 mixture of a PI and Hoechst 33342 dye to confirm that the cell death resulted from the CPT release. A cell viability assay showed that cell survival decreased about to half after 10 min of the impeller excitation with ~ 0.1 W/cm^2 at 413 nm.

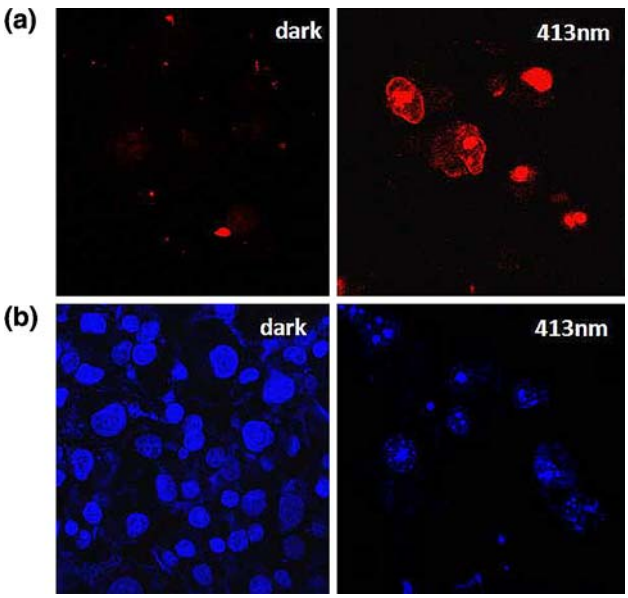

Fig. 9 Confocal fluorescence images of the PANC-1 cancer cells that were treated with a suspension of the particles loaded with the (**a**) PI or (**b**) CPT, and kept in the dark (left column) and illuminated for 5 minutes with 413 nm light (right column)

7 Summary

In this paper we have discussed several recent advances in light-activated functional mesoporous silica. Using CTAB templated silica thin films, spatial separation of energy donors and acceptors as well as electron donors and acceptors was achieved. Steady state and time resolved luminescence spectroscopy were used to prove that spatial separation of donors and acceptors was achieved using deliberate placement strategies. Calculations based on Förster theory were used to further demonstrate spatial separation by determining a minimum separation distance between donors and acceptors that is close to the dimensions of the mesostructured thin films. Photo-induced electron transfer studies were carried out with spatially separated donors and acceptors, where the spatial separation was again verified by luminescence spectroscopy. Two important quantities, the contact quenching rate and the electron tunneling decay coefficient, were calculated, and mesostructured silica was compared to a number of other materials and systems including frozen liquids and proteins. Mesostructured silica is an excellent insulator.

Mesostructured particles are also important frameworks for molecular machines. Light activated trapping and release of molecules from the pores was accomplished using molecular machines and impellers. Parallel to the development of controlled release systems, biologically compatible particles were synthesized and dye molecules from pores inside of living cells were released under remote control. Functional mesostructured silica made by sol–gel methods and derivatized with active molecules provide a versatile family of materials for both fundamental physical studies and biological applications.

Acknowledgments This work was made possible by grants from the US National Science Foundation (CHE 0507929, DMR 0346601), and FENA. The authors acknowledge the contributions by the many co-workers whose accomplishments are cited in the references.

References

1. Brinker CJ, Scherer GW (1990) Sol–gel science: the physics and chemistry of sol–gel processing. Academic Press Inc., San Diego
2. Loy DA, Shea KJ (1995) Chem Rev 95:1431
3. Soler-Illia GJD, Sanchez C, Lebeau B, Patarin J (2002) Chem Rev 102:4093
4. Avnir D, Braun S, Lev O, Ottolenghi M (1994) Chem Mater 6:1605
5. Avnir D (1995) Acc Chem Res 28:328
6. Ellerby LM, Nishida CR, Nishida F, Yamanaka SA, Dunn B, Valentine JS, Zink JI (1992) Science 255:1113
7. Dave BC, Dunn B, Valentine JS, Zink JI (1994) Anal Chem 66:A1120
8. Miller JM, Dunn B, Valentine JS, Zink JI (1996) J Non-Crystalline Solids 202:279
9. Lan EH, Dunn B, Zink JI (2000) Chem Mater 12:1874

10. Dave BC, Miller JM, Dunn B, Valentine JS, Zink JI (1997) J Sol–Gel Sci Tech 8:629
11. Chia SY, Urano J, Tamanoi F, Dunn B, Zink JI (2000) J Am Chem Soc 122:6488
12. Kresge CT, Leonowicz ME, Roth WJ, Vartuli JC, Beck JS (1992) Nature 359:710
13. Lu YF, Ganguli R, Drewien CA, Anderson MT, Brinker CJ, Gong WL, Guo YX, Soyez H, Dunn B, Huang MH, Zink JI (1997) Nature 389:364
14. Huo QS, Margolese DI, Ciesla U, Feng PY, Gier TE, Sieger P, Leon R, Petroff PM, Schuth F, Stucky GD (1994) Nature 368:317
15. Zhao DY, Yang PD, Huo QS, Chmelka BF, Stucky GD (1998) Curr Opin Solid St M 3:111
16. Bartl MH, Boettcher SW, Frindell KL, Stucky GD (2005) Acc Chem Res 38:263
17. Huo QS, Margolese DI, Ciesla U, Demuth DG, Feng PY, Gier TE, Sieger P, Firouzi A, Chmelka BF, Schuth F, Stucky GD (1994) Chem Mater 6:1176
18. Hernandez R, Franville AC, Minoofar P, Dunn B, Zink JI (2001) J Am Chem Soc 123:1248
19. Minoofar PN, Hernandez R, Chia S, Dunn B, Zink JI, Franville AC (2002) J Am Chem Soc 124:14388
20. Minoofar P, Hernandez R, Franville AC, Chia SY, Dunn B, Zink JI (2003) J Sol–Gel Sci Tech 26:571
21. Minoofar PN, Dunn BS, Zink JI (2005) J Am Chem Soc 127:2656
22. Huang MH, Dunn BS, Soyez H, Zink JI (1998) Langmuir 14:7331
23. Huang MH, Dunn BS, Zink JI (2000) J Am Chem Soc 122:3739
24. Huang MH, Soyez HM, Dunn BS, Zink JI (2000) Chem Mater 12:231
25. Franville AC, Dunn B, Zink JI (2001) J Phys Chem B 105:10335
26. Johansson E, Zink JI (2007) J Am Chem Soc 129:14437
27. Huang MH, Kartono F, Dunn B, Zink JI (2002) Chem Mater 14:5153
28. Ford C, Singh M, Lawson L, He JB, John V, Lu YF, Papadopoulos K, McPherson G, Bose A (2004) Colloids Surf B 39:143
29. Corriu RJP, Mehdi A, Reye C (2005) J Mater Chem 15:4285
30. Corriu RJP, Mehdi A, Reye C, Thieuleux C (2002) Chem Commun 1382
31. Okamoto K, Kapoor MP, Inagaki S (2005) Chem Comm 1423
32. Inagaki S, Guan S, Ohsuna T, Terasaki O (2002) Nature 416:304
33. Kapoor Mahendra P, Yang Q, Inagaki S (2002) J Am Chem Soc 124:15176
34. Nicole L, Boissiere C, Grosso D, Quach A, Sanchez C (2005) J Mater Chem 15:3598
35. Sierocki P, Maas H, Dragut P, Richardt G, Vogtle F, Cola L, Brouwer FAM, Zink JI (2006) J Phys Chem B 110:24390
36. Corriu RJP, Lancelle-Beltran E, Mehdi A, Reye C, Brandes S, Guilard R (2002) J Mater Chem 12:1355
37. Yui T, Tsuchino T, Itoh T, Ogawa M, Fukushima Y, Takagi K (2005) Langmuir 21:2644
38. Angelos S, Choi E, Vogtle F, De Cola L, Zink JI (2007) J Phys Chem C 111:6589
39. Nguyen TD, Tseng HR, Celestre PC, Flood AH, Liu Y, Stoddart JF, Zink JI (2005) Proc Natl Acad Sci USA 102:10029
40. Thomas A, Polarz S, Antonietti M (2003) J Phys Chem B 107:5081
41. Renge I (2000) J Phys Chem A 104:7452
42. Bojarski C, Obermueller G (1976) Acta Physica Polonica A 50:389
43. Jones G (1990) In: Duarte FJ, Hillman LW (eds) Dye laser principles with applications. Academic Press, San Diego, p 287
44. del Monte F, Mackenzie JD, Levy D (2000) Langmuir 16:7377
45. Lee CW, Oh MK, Jang JM (1993) Langmuir 9:1934
46. Brugger PA, Infelta PP, Braun AM, Gratzel M (1981) J Am Chem Soc 103:320
47. Miller JR, Beitz JV (1981) J Chem Phys 74:6746
48. Ponce A, Gray HB, Winkler JR (2000) J Am Chem Soc 122:8187
49. Smalley JF, Finklea HO, Chidsey CED, Linford MR, Creager SE, Ferraris JP, Chalfant K, Zawodzinsk T, Feldberg SW, Newton MD (2003) J Am Chem Soc 125:2004
50. Wenger OS, Leigh BS, Villahermosa RM, Gray HB, Winkler JR (2005) Science 307:99
51. Hernandez R, Tseng HR, Wong JW, Stoddart JF, Zink JI (2004) J Am Chem Soc 126:3370
52. Leung KCF, Nguyen TD, Stoddart JF, Zink JI (2006) Chem Mater 18:5919
53. Nguyen TD, Leung KCF, Liong M, Pentecost CD, Stoddart JF, Zink JI (2006) Org Lett 8:3363
54. Saha S, Leung KCF, Nguyen TD, Stoddart JF, Zink JI (2007) Adv Funct Mater 17:685
55. Nguyen TD, Liu Y, Saha S, Leung KCF, Stoddart JF, Zink JI (2007) J Am Chem Soc 129:626
56. Park C, Oh K, Lee SC, Kim C (2007) Angew Chem Int Ed 46:1455
57. Lai CY, Trewyn BG, Jeftinija DM, Jeftinija K, Xu S, Jeftinija S, Lin VSY (2003) J Am Chem Soc 125:4451
58. Alvaro M, Benitez M, Das D, Garcia H, Peris E (2005) Chem Mater 17:4958
59. Besson E, Mehdi A, Lerner DA, Reye C, Corriu RJP (2005) J Mater Chem 15:803
60. Liu N, Dunphy DR, Atanassov P, Bunge SD, Chen Z, Lopez GP, Boyle TJ, Brinker CJ (2004) Nano Lett 4:551
61. Liu NG, Dunphy DR, Rodriguez MA, Singer S, Brinker J (2003) Chem Comm 1144
62. Huh S, Wiench JW, Yoo JC, Pruski M, Lin VSY (2003) Chem Mater 15:4247
63. Munoz B, Ramila A, Perez-Pariente J, Diaz I, Vallet-Regi M (2003) Chem Mater 15:500
64. Han YJ, Stucky GD, Butler A (1999) J Am Chem Soc 121:9897
65. Stein A, Melde BJ, Schroden RC (2000) Adv Mater 12:1403
66. Lu J, Liong M, Zink JI, Tamanoi F (2007) Small 3:1341
67. Cai Q, Luo ZS, Pang WQ, Fan YW, Chen XH, Cui FZ (2001) Chem Mater 13:258
68. Radu DR, Lai CY, Jeftinija K, Rowe EW, Jeftinija S, Lin VSY (2004) J Am Chem Soc 126:13216
69. Lin YS, Tsai CP, Huang HY, Kuo CT, Hung Y, Huang DM, Chen YC, Mou CY (2005) Chem Mater 17:4570
70. Santra S, Yang H, Dutta D, Stanley JT, Holloway PH, Tan W, Moudgil BM, Mericle RA (2004) Chem Comm 2810
71. Bagwe RP, Hilliard LR, Tan W (2006) Langmuir 22:4357
72. Lu J, Choi E, Tamanoi F, Zink JI (2007) In Press